



HAL
open science

Tm,Ho:Ca(Gd,Lu)AlO₄ crystals: Crystal growth, structure refinement and Judd-Ofelt analysis

Zhongben Pan, Pavel Loiko, Sami Slimi, Hualei Yuan, Yicheng Wang, Yongguang Zhao, Patrice Camy, Elena Dunina, Alexey Kornienko, Liudmila Fomicheva, et al.

► To cite this version:

Zhongben Pan, Pavel Loiko, Sami Slimi, Hualei Yuan, Yicheng Wang, et al.. Tm,Ho:Ca(Gd,Lu)AlO₄ crystals: Crystal growth, structure refinement and Judd-Ofelt analysis. *Journal of Luminescence*, 2022, 246, pp.118828. 10.1016/j.jlumin.2022.118828 . hal-03858700

HAL Id: hal-03858700

<https://hal.science/hal-03858700>

Submitted on 17 Nov 2022

HAL is a multi-disciplinary open access archive for the deposit and dissemination of scientific research documents, whether they are published or not. The documents may come from teaching and research institutions in France or abroad, or from public or private research centers.

L'archive ouverte pluridisciplinaire **HAL**, est destinée au dépôt et à la diffusion de documents scientifiques de niveau recherche, publiés ou non, émanant des établissements d'enseignement et de recherche français ou étrangers, des laboratoires publics ou privés.

Tm,Ho:Ca(Gd,Lu)AlO₄ crystals: Part I. Crystal growth, structure refinement and Judd-Ofelt analysis

Zhongben Pan^{1,2}, Pavel Loiko³, Sami Slimi⁴, Hualei Yuan¹, Xiaojun Dai¹, Huaqiang Cai¹, Yicheng Wang², Yongguang Zhao^{2,5}, Patrice Camy³, Elena Dunina⁶, Alexey Kornienko⁶, Liudmila Fomicheva⁷, Weidong Chen^{2,8}, Uwe Griebner², Valentin Petrov², Rosa Maria Solé⁴, Francesc Díaz⁴, Magdalena Aguiló⁴, and Xavier Mateos^{4,9,*}

¹*Institute of Chemical Materials, China Academy of Engineering Physics, Mianyang, 621900, China*

²*Max Born Institute for Nonlinear Optics and Short Pulse Spectroscopy, Max-Born-Str. 2a, 12489 Berlin, Germany*

³*Centre de Recherche sur les Ions, les Matériaux et la Photonique (CIMAP), UMR 6252 CEA-CNRS-ENSICAEN, Université de Caen Normandie, 6 Boulevard du Maréchal Juin, 14050 Caen Cedex 4, France*

⁴*Universitat Rovira i Virgili, Dept. Química Física i Inorgànica, FiCMA-FiCNA-EMaS, Marcel·li Domingo, 1, 43007 Tarragona, Spain*

⁵*Jiangsu Key Laboratory of Advanced Laser Materials and Devices, Jiangsu Normal University, 221116 Xuzhou, China*

⁶*Vitebsk State Technological University, 72 Moskovskaya Ave., 210035 Vitebsk, Belarus*

⁷*Belarusian State University of Informatics and Radioelectronics, 6 Brovka St., 220027, Minsk, Belarus*

⁸*Key Laboratory of Optoelectronic Materials Chemistry and Physics, Fujian Institute of Research on the Structure of Matter, Chinese Academy of Sciences, Fuzhou, 350002 Fujian, China*

⁹*Serra Hùnter Fellow*

*Corresponding author: xavier.mateos@urv.cat

ABSTRACT. “Mixed” calcium rare-earth aluminate laser host crystals Ca(Gd,Lu)AlO₄ with up to 10.8 at.% Lu codoped with Tm³⁺ and Ho³⁺ ions are grown by the Czochralski method along the [001] direction. The segregation of rare-earth ions is studied. The crystal structure is refined by the Rietveld method. Tm,Ho:Ca(Gd,Lu)AlO₄ crystallizes in the tetragonal system (sp. gr. *I4/mmm*) exhibiting a K₂NiF₄ type structure. The lattice constants are $a = 3.6585$ (6) Å and $c = 11.9660$ (9) Å for a crystal with a composition of CaGd_{0.8327}Lu_{0.108}Tm_{0.0555}Ho_{0.0038}AlO₄. The stability of Ca(Gd,Lu)AlO₄ solid-solutions is discussed. The polarized Raman spectra are measured, revealing a most intense mode at 311 cm⁻¹ and a maximum phonon frequency of ~650 cm⁻¹. The polarized absorption spectra are measured. The transition intensities for the Ho³⁺ ion are analyzed using the modified Judd-Ofelt theory accounting for configuration interaction.

Keywords: Aluminate crystals; Czochralski growth; Structure refinement; Raman spectra; Optical absorption; Judd-Ofelt theory.

1. Introduction

Calcium rare-earth aluminates CaLnAlO_4 where Ln stands for Gd or Y (denoted as CALGO / CGA and CALYO / CYA, respectively) are attractive laser host crystals [1-3]. They crystallize in a tetragonal class having a K_2NiF_4 -type structure and exhibit structural disorder: the Ca^{2+} and Ln^{3+} cations are statistically distributed over the same Wyckoff site (4e, C_{4v} -symmetry) [4,5]. As a result, CaLnAlO_4 doped with laser-active trivalent rare-earth ions (RE^{3+}) such as Yb^{3+} , Tm^{3+} , Ho^{3+} , etc., exhibit significant inhomogeneous broadening of spectral bands [6]. Despite their disordered nature, the CaLnAlO_4 crystals provide good thermal properties, such as high thermal conductivity ($\sim 6.7 \text{ Wm}^{-1}\text{K}^{-1}$ for CaGdAlO_4) with moderate dependence on the RE^{3+} doping concentration, weak anisotropy of thermal expansion and negative thermo-optic coefficients leading to almost “athermal” behavior [7]. Tetragonal CaLnAlO_4 crystals exhibit natural birefringence [8] and enable polarized laser emission [9]. Due to the presence of the substitutional rare-earth site, the doping of CaLnAlO_4 crystals is relatively easy. Finally, particularly for Ln = Gd and Y, the CaLnAlO_4 compounds melt congruently (at $\sim 1750 \text{ }^\circ\text{C}$ in the former case), so that large crystals can be grown relatively easy by the conventional Czochralski (Cz) method [10].

The reported thermal and spectroscopic properties of RE^{3+} -doped CaLnAlO_4 rendered these crystals excellent candidates for generation and amplification of ultrashort laser pulses [11,12], including the high-power regime [13] (e.g., thin-disk lasers [14,15]). In the past decades, the research activity mainly focused on Yb^{3+} -doped crystals corresponding to the spectral range of $\sim 1 \text{ } \mu\text{m}$ [11-15]. More recently, the interest shifted towards the eye-safe spectral range of $\sim 2 \text{ } \mu\text{m}$ [16,17]. The laser emission at $\sim 2 \text{ } \mu\text{m}$ is typically achieved using thulium (Tm^{3+}) and / or holmium (Ho^{3+}) dopant ions. The growth and spectroscopic characterization of singly doped and $\text{Tm}^{3+}, \text{Ho}^{3+}$ -codoped CaGdAlO_4 and CaYAlO_4 crystals were reported in [3,18]. Furthermore, such materials were proven to be capable of generating femtosecond pulses at $\sim 2 \text{ } \mu\text{m}$ [16,17].

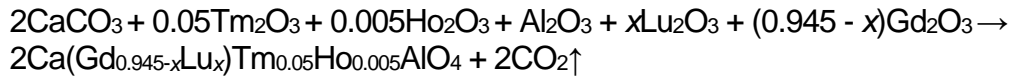
The CaLnAlO_4 crystals belong to a big class of oxides with a general chemical formula of ABCO_4 , where $\text{A}^{2+} = \text{Ca}^{2+}$ or Sr^{2+} , B^{3+} is a rare-earth cation, and $\text{C}^{3+} = \text{Al}^{3+}$ or Ga^{3+} [19]. Not all the possible ABCO_4 compositions are stable, exhibit the desired K_2NiF_4 -type tetragonal structure and melt congruently. Other known compositions satisfying these conditions are SrLaAlO_4 and SrLaGaO_4 [20,21]. The search for other compositions of ABCO_4 crystals (and, in particular, CaLnAlO_4 ones) will help to improve the thermal and spectroscopic properties. Another option is the growth of “mixed” crystals (solid solutions) leading to compositional disorder and hence to additional broadening of the spectral bands of laser-active RE^{3+} dopant ions. As for the CaLnAlO_4 crystals, the Cz growth of stoichiometric compounds with other host-forming Ln^{3+} cations was reported only for Ln = Nd [4], Dy [23] and Tb [24]. However, all these ions are optically active and do not appear attractive for “mixed” crystals.

The lutetium ion (Lu^{3+}) is known as a passive host-forming cation for many oxide materials such as garnets ($\text{Lu}_3\text{Al}_5\text{O}_{12}$), sesquioxides (Lu_2O_3), tungstates ($\text{KLu}(\text{WO}_4)_2$) or perovskites (LuAlO_3). Due to the closeness of ionic radii of Lu^{3+} and Yb^{3+} or Tm^{3+} ions, Lu-based oxides (as compared to their Gd-based counterparts) provide easier doping and weaker dependence of thermal properties on the doping level [25]. Unfortunately, so far, the CaLuAlO_4 compound has never been synthesized as a single crystal [26]. An alternative route can be the fabrication of a “mixed” material, e.g., $\text{Ca}(\text{Gd},\text{Lu})\text{AlO}_4$ with a partial substitution of Gd^{3+} by Lu^{3+} . First, this idea was exploited in [27] to produce Yb^{3+} -doped $\text{Ca}(\text{Gd},\text{Lu})\text{AlO}_4$ crystals (denoted as CLGA) with a maximum Lu^{3+} content of 5.5 at.%. Later, Tm^{3+} -doped crystals with a similar Lu^{3+} content were grown and their spectroscopic and laser properties were studied [28].

In the present work, we report on the first Cz growth of Tm³⁺,Ho³⁺-codoped “mixed” Ca(Gd,Lu)AlO₄ crystals preserving the tetragonal K₂NiF₄-type structure. These crystals feature increased Lu³⁺ content up to 10.8 at.% extending the understanding of solid-solution formation in the system Ca(Gd_{1-x}Lu_x)AlO₄.

2. Crystal growth

5 at.% Tm³⁺, 0.5 at.% Ho³⁺ (in the melt) codoped Ca(Gd_{1-x}Lu_x)AlO₄ (where $x = 0.1$ or 0.2 corresponds to batches #1 and #2, respectively) single crystals were grown by the Cz method using an argon atmosphere in an iridium crucible. An automatic system was employed to control the boule diameter. The polycrystalline materials were obtained by solid-state reaction from a mixture of the starting materials, Al₂O₃, RE₂O₃ (where RE = Gd, Lu, Tm and Ho) (purity: 5N) and CaCO₃ (purity: 4N). For that, the raw materials taken in stoichiometric composition according to the following formula were well mixed, ground and firstly heated to 1173 K for 12 hours (h) to decompose CaCO₃ using a platinum crucible. Once the crucible was cooled down to room temperature, the obtained mixture was pressed into pellets and again reheated to 1673 K for 30 h to synthesize polycrystalline materials.



The synthesized polycrystalline material was placed in an iridium crucible and melted by an intermediate-frequency heater. A [001]-oriented undoped CaGdAlO₄ seed was used, the pulling rate varied from 0.5 to 2 mm/h and the crystal rotation speed was kept at 8 to 15 revolutions per minute (rpm). Once the growth was completed, the crystals were removed from the melt and slowly cooled down to room temperature (RT, 293 K) at a stepped rate of 15 to 25 K/h. The photographs of the as-grown crystal boules of Tm,Ho:Ca(Gd,Lu)AlO₄ are shown in Fig. 1(a,c). They have a cylindrical shape with slightly varying cross-section along the length of the boule (about 3.0 cm). The as-grown crystals exhibit brown-yellow coloration which is typical for aluminate crystals [29-31] and is assigned to interstitial oxygen ions. The crystal boules with high Lu³⁺ content show some small cracks at their shoulders. We attribute this to the flat shape of the shoulders, which causes much larger radiant area during the crystal growth and cooling process. Though small cracks exist in the crystal, the samples cut from the crystal are still of high optical quality. The coloration is greatly removed by annealing at 950°C for 24 h under N₂ atmosphere with 5% H₂ (in oxygen-deficient conditions).

2. Experimental

The concentration of doping ions (Tm³⁺, Ho³⁺ and Lu³⁺) was measured by Inductively Coupled Plasma Mass Spectrometry (ICP-MS) using an Agilent® 8800 triple quadrupole ICP-MS analyzer.

The X-ray powder diffraction (XRD) patterns were measured at RT using a Bruker D2 Phaser diffractometer for diffraction angles 2θ in the range of 10 - 90° with Cu Kα1 radiation (1.54051 Å).

The crystal density was measured by the buoyancy method at 294 K, $\rho_{\text{meas}} = (m\rho_{\text{water}})/(m - m')$, where m and m' is the sample mass in air and in water, respectively, $\rho_{\text{water}} = 0.998 \text{ g/cm}^3$ is the density of water. Each ρ_{meas} value was averaged for 3 different samples from the same batch.

For polarized Raman and absorption measurements, rectangular samples oriented along the crystallographic axes (**a**, **c**) were prepared and polished (all lateral sides), as

shown in Fig. 1(b,d). The polarized Raman spectra were measured using a confocal Raman microscope (Renishaw inVia) equipped with a $\times 50$ objective, a set of a polarizer, an analyzer and a $\lambda/2$ plate, and a cut-on filter. The excitation wavelength was 514 nm (Ar⁺ ion laser line).

The RT polarized absorption spectra in the range of 300-2200 nm were measured using a CARY 5000 (Varian) spectrophotometer equipped with a Glan-Taylor polarizer; the resolution (spectral bandwidth, SBW) was 0.2 nm.

3. Structural study

3.1. Crystal composition

The results on the concentration of doping ions (Tm³⁺, Ho³⁺ and Lu³⁺) are shown in Table 1. In particular, for batch #1, the actual doping levels were determined to be 4.48 at.% Tm, 0.54 at.% Ho and 5.51 at.% Lu corresponding to the stoichiometric chemical formula of CaGd_{0.8946}Lu_{0.055}Tm_{0.045}Ho_{0.0054}AlO₄. The ion densities amounted to $N_{\text{Tm}} = 5.54 \times 10^{20} \text{ cm}^{-3}$ and $N_{\text{Ho}} = 0.66 \times 10^{20} \text{ cm}^{-3}$.

Let us analyze the segregation coefficients for three rare-earth ions, $K_{\text{RE}} = C_{\text{crystal}}/C_{\text{melt}}$, where C_{crystal} and C_{melt} are the doping levels in the crystal and in the raw materials (in the melt), respectively. For Tm³⁺ and Ho³⁺ ions, they are close to unity, $K_{\text{Tm}} = 0.90$ and $K_{\text{Ho}} = 0.76 - 1.07$ and for Lu³⁺ ones, $K_{\text{Lu}} = 0.54 - 0.55$ is much smaller. In the parent compound, CaGdAlO₄, the host-forming Ca²⁺ and Gd³⁺ cations statistically occupy the same type of site (Wyckoff symbol: 4e, site symmetry: C_{4v}, coordination number (C.N.) by oxygen: IX). It is expected that all the dopant cations replace for the Gd³⁺ ones. The observed difference in the segregation coefficients can be understood from the point of view of mismatch of ionic radii, namely $R_{\text{Tm}} = 1.052 \text{ \AA}$, $R_{\text{Ho}} = 1.072 \text{ \AA}$ and $R_{\text{Lu}} = 1.032 \text{ \AA}$, compared with the larger $R_{\text{Gd}} = 1.107 \text{ \AA}$ and especially $R_{\text{Ca}} = 1.180 \text{ \AA}$ [32]. The results are compiled also in Fig. 2 where data on K_{RE} for other rare-earth ions in CaGdAlO₄ crystals from the literature [33-38] are added. The data were fitted using the following formula based on Onuma's principle [39]: $K_{\text{RE}} = K_0 - C(R_{\text{RE}} - R_{\text{Gd}})^2$ with the best-fit parameters $K_0 = 1.1 \pm 0.1$ and $C = 95 \pm 5 \text{ \AA}^{-2}$.

It is known that a solid-solution of isostructural compounds can be formed if the relative difference between the ionic radii of the host-forming cation H (Gd³⁺, in our case) and the dopants D (Lu³⁺, Tm³⁺, Ho³⁺, ion our case), expressed by the formula $\Delta_{\text{R}} = |(R_{\text{D}} - R_{\text{H}})/R_{\text{H}}| \times 100\%$, does not exceed 15%. In our case, this parameter is maximum for Lu³⁺, $\Delta_{\text{R}} = 6.8\%$, but the above-mentioned condition is still satisfied.

3.2. X-ray diffraction

The measured X-ray powder diffraction (XRD) patterns of the Tm,Ho:Ca(Gd,Lu)AlO₄ crystals are shown in Fig. 3. In the same figure, we show the theoretical reflections from the Crystallography Open Database (COD) card #96-722-7258 for undoped CaGdAlO₄. The experimental XRD patterns match well the theoretical ones, indicating a single-phase nature of the material. The crystal structure was refined using the Rietveld method with the aim of the *match!* software, as shown in Fig. 4. The atomic coordinates from [30] were taken as a starting model for the Rietveld refinement. The obtained main crystallographic data and the refinement parameters are listed in Table 2. Tm,Ho:Ca(Gd,Lu)AlO₄ crystallizes in the tetragonal system (sp. gr. D_{4h}¹⁷ - *I4/mmm*, No. 139) exhibiting a K₂NiF₄ type structure. For the crystal growth from the batch #1, the lattice constants $a = b = 3.6585(6) \text{ \AA}$, $c = 11.9660(9) \text{ \AA}$, the volume of the unit-cell $V = 160.167 \text{ \AA}^3$ (number of the formula units per unit-cell $Z = 2$). The calculated crystal density is then $\rho_{\text{calc}} = 6.010 \text{ g/cm}^3$. The measured density ρ_{meas} amounted to 6.02 g/cm^3 (batch #1) and 6.08 g/cm^3 (batch #2), respectively, in agreement with the values calculated from the XRD data. The obtained lattice constants are slightly smaller than those for undoped CaGdAlO₄, $a = 3.6632(3) \text{ \AA}$

and $c = 11.998(2)$ Å [30], because of the smaller ionic radii of the dopant cations as compared to the host-forming ones.

The reliability factors obtained are listed in Table 2. For the crystal grown from batch #1, the weighted profile R -factor $R_{wp} = 2.82$, the expected R -factor $R_{exp} = 2.31$ and the Chi-squared $\chi^2 = (R_{wp}/R_{exp})^2 = 3.33$.

The fractional atomic coordinates, the occupancy factors (O.F.) and the isotropic displacement parameters (B_{iso}) determined during the refinement are listed in Table 3. For the 4e sites, we assumed a random distribution of Ca^{2+} and RE^{3+} cations following the ratio of 1:1. The O.F. of the RE^{3+} ions (Gd^{3+} , Lu^{3+} , Tm^{3+} and Ho^{3+}) were taken according to the determined actual crystal compositions, Table 1.

A fragment of the crystal structure drawn using the VESTA software according to the determined set of atomic coordinates is shown in Fig. 5. The corresponding interatomic distances (Al – O, Ca|RE – O and Ca|RE – Ca|RE) are summarized in Table 4. Al^{3+} cations are located in 2a sites (symmetry: C_{4v}) and they are VI-fold oxygen coordinated forming distorted $[AlO_6]$ octahedra elongated along the [001] direction. The distances from Al to two axial O1 atoms are 2.028(4) Å and thus longer than the “ideal” Al–O bond length (1.935 Å), whereas the distances to the four basal O2 atoms are 1.829(2) Å and thus shorter than the “ideal” bond length (here and below, the distances are specified for batch #1), Fig. 6. The Ca^{2+} | RE^{3+} cations statistically occupy the 4e sites (symmetry: C_{4v}) and they are IX-fold oxygen coordinated. There is one shorter (O1, 2.276(9) Å), four intermediate (O2, 2.482(0) Å) and four longer (O1' 3.687(5) Å) distances in the $[Ca|REO_9]$ polyhedra, Fig. 6, leading to a mono-capped tetragonal anti-prismatic geometry. The oxygen atoms are distributed over the 4e (O1) and 4c (O2) sites.

The structure of $Tm, Ho:Ca(Gd, Lu)AlO_4$ is determined by a condensed framework of corner-sharing $[AlO_6]$ and $[Ca|REO_9]$ polyhedra. They form infinite layers parallel to the a – b plane. More generally, the structure of tetragonal (K_2NiF_4 -type) $ABCO_4$ crystals can be divided into a sequence of layers running along the [001] direction with rock salt (S) and perovskite (P) structure [40]. In the case of $Tm, Ho:Ca(Gd, Lu)AlO_4$, the P and S “phases” comprise $REAlO_3$ and CaO , respectively.

In Fig. 7, we analyze the Al – O interatomic distances in $[AlO_6]$ octahedra for various $MM'AlO_4$ crystals possessing the tetragonal K_2NiF_4 -type structure [4]. The distances to axial and basal O atoms, as well as their average values increase with the mean ionic radius of the M^{2+} and M^{3+} cations, so that the average distance approaches the “ideal” value of 1.935 Å, calculated from the ionic radii of VI-fold coordinated Al^{3+} (0.535 Å) and O^{2-} (1.40 Å) [32] (typically, the Al – O distances are invariant [4]). This distortion of the $[AlO_6]$ octahedra occurs as the Al – O2 bond distance is constrained by the unit-cell dimensions (both Al and O2 are located in special positions, Table 3), while the Al – O1 distances are constrained by the lattice constant c and the variable z atomic coordinate.

The second coordination sphere of Ca^{2+} | RE^{3+} cations is composed of 9 nearest neighbor 4e sites, Fig. 8. The shortest metal-to-metal Ca|RE – Ca|RE distance is 3.355(2) Å ($\times 1$), observed along the $[u\ v\ w] = [001]$ direction. Other interactions correspond to intermediate distances of 3.658(5) Å ($\times 4$) and longest distances of 3.687(5) Å $\times 4$. The origin of the disorder is the second coordination sphere of RE^{3+} ions, namely the charge difference between the Ca^{2+} and RE^{3+} cations and the large difference in the metal-to-metal distances [6]. As only one apical site corresponds to the shortest Ca|RE – Ca|RE distance, it induces two families of local environment if it is occupied by Ca^{2+} or RE^{3+} cations. Each family contains surroundings with different distributions of Ca^{2+} and RE^{3+} cations over eight remaining 4e sites. This leads to significant inhomogeneous broadening of the spectral bands of optically active RE^{3+} cations. The introduction of Lu^{3+} further enhances the disorder, considering the difference in the ionic radii of Lu^{3+} and Gd^{3+} .

It is worth discussing the expected effect of RE³⁺ ions on the spectral line broadening. One may argue that the addition of optically active dopants (Tm³⁺ or Ho³⁺) in high concentrations by itself can induce an additional “compositional” disorder. However, the doping level for both ions is limited by the detrimental energy-transfer upconversion capable of preventing the desired laser operation. In the (Tm³⁺, Ho³⁺) system, an optimum codoping ratio Ho/Tm between 1:10 and 1:5 is required to ensure a unidirectional Tm³⁺ → Ho³⁺ energy-transfer. These spectroscopic considerations limit in practice the actual doping levels for both ions. The Lu³⁺ cations are optically passive and thus do not induce unwanted spectroscopic processes. Moreover, the difference in the ionic radii in the pair Gd³⁺ | Lu³⁺ is larger than in the pairs Gd³⁺ | Tm³⁺, Ho³⁺ which enhances the additional spectral broadening. The drawback is the lower segregation coefficient for Lu³⁺.

Let us also discuss the terminological aspect of calling the grown crystals “mixed”. Strictly speaking, they should be called a substitutional single-phase solid solution. The term “mixed” crystal exists as a synonym to solid solution materials, e.g., A_{1-x}B_x if there are only two parent compounds. As explained above, we assume that Tm³⁺ and Ho³⁺ as dopants hardly affect the spectral broadening, while Lu³⁺ is the cation aimed to fulfil this task. There is no universal definition for the x parameter in A_{1-x}B_x to distinguish the term “doping” from the “mixed” crystal or solid-solution. From the point of view of optics, the borderline can be defined as the minimum value inducing a noticeable change on the spectroscopic properties. As will be shown in Part II of this work, this condition is satisfied in the grown crystals, so that the Lu³⁺ doping level is about x = 0.05 - 0.1, i.e., the compositions Ca(Gd_{0.9-0.95}Lu_{0.1-0.05})AlO₄ can be taken as the lower limit of the solid-solution definition.

It is not clear yet what is the upper limit (x) for the existence of such a solid solution. The single crystal growth of CaLuAlO₄ has never been reported in the literature. In [26], the author attempted to grow CaLuAlO₄ using the standard procedure for CaGdAlO₄ resulting in polycrystalline, fine-grained, needle-like body of orange-red color with only the cubic Lu₂O₃ structure reliably identified. He concluded that CaLuAlO₄, if it exists at all, melts incongruently and the phase relationships in the CaO-Lu₂O₃-Al₂O₃ system differ greatly from those for the CaO-Gd₂O₃-Al₂O₃ one.

The stability of ABCO₄ crystals can be assessed from the following considerations. The ionic radii of the A²⁺ and B³⁺ cations provide the information about the deviation from the ideal perovskite lattice (for the P “phase”). Such a deviation will cause deformations in and between the P and S “phase” layers. For BCO₃ crystals with a perovskite structure, the so-called Goldschmidt's tolerance factor *t* is given by [41]:

$$t = \frac{R(B^{3+}) + R(O^{2-})}{\sqrt{2}(R(C^{3+}) + R(O^{2-}))}. \quad (1)$$

Taking into account the statistical distribution of A²⁺ and C³⁺ cations in the tetragonal ABCO₄ crystals, we should replace $R(B^{3+})$ by $(R(A^{2+}) + R(B^{3+}))/2$ in Eq. 1. Liebold estimated the following range of tolerance factors for which the tetragonal structure is stable [26]: $0.92 < t < 0.95$. For CaGdAlO₄ and CaYAlO₄ crystals, $t = 0.9295$ and 0.9236 , respectively, i.e., well satisfying this condition, while for hypothetically existing CaLuAlO₄, $t = 0.9157$. From Eq. (1), modified for the case of ABCO₄ crystals and the above mentioned range for tolerance factors, we estimate the maximum content of Lu³⁺ in the CaGd_{1-x}Lu_xAlO₄ solid solution as $x = 0.7$. While this is a rough estimation, we expect that stable solid-solutions with Lu³⁺ content up to few tens of at.% may exist.

3.3. Raman spectroscopy

The factor group analysis [42] for the primitive cell of the D_{17h}⁴ symmetry predicts the following set of irreducible representations at the center of the Brillouin zone ($\mathbf{k} = 0$): $\Gamma = 2A_{1g} + 2E_g + 4A_{2u} + 5E_u + B_{2u}$ [43]. Four Raman active modes are all even species involving

vibrations of mainly one type of atoms: $A_{1g} + E_g$ modes of Ca|RE and $A_g + E_g$ modes of O; 11 IR-active modes are $3A_{2u} + 4E_u$; two modes ($A_{2u} + E_u$) are acoustic and one (B_{2u}) is silent [43,44].

The polarized Raman spectra of the Tm,Ho:Ca(Gd,Lu)AlO₄ crystal (batch #1) are shown in Fig. 9. They were measured using both **a**-cut and **c**-cut samples. In Fig. 9, we use Porto's notations [45]: $m(nk)\bar{l}$, where m and l are the directions of propagation of the incident and scattered light, respectively (in our case for the confocal geometry, $m \equiv l$), and n and k are the polarization states of the incident and scattered light, respectively. Thus, five spectra were measured, $a(nk)\bar{a}$, where $n, k = \pi$ or σ and $c(\sigma\sigma)\bar{c}$. The Raman spectra are strongly polarized.

In the spectra taken for **a**-cut crystals, all the Raman-active modes should appear: the $a(\pi\pi)\bar{a}$ geometry selects the A_{1g} phonons, and in the $a(\pi\sigma)\bar{a}$ geometry, the E_g modes appear. For the E_g geometry, as expected, only two intense modes at ~ 154 and 313 cm^{-1} appear [43]. The low-frequency mode is assigned to Ca|RE vibrations in the **a-b** plane and the high-frequency one – to the similar O vibrations. For the $a(\sigma\sigma)\bar{a}$ A_{1g} geometry, another band at even higher frequencies with two maxima, at 514 and 542 cm^{-1} , appears and it is assigned to O vibrations. For the $a(\pi\pi)\bar{a}$ A_{1g} geometry, the spectrum presents the most intense band at 311 cm^{-1} and a weaker band at ~ 542 cm^{-1} . The band at ~ 311 cm^{-1} is thus assigned to A_{1g} symmetry (Ca|RE vibrations along the **c**-axis) and the band with a complex structure (clearly revealed for the $a(\sigma\sigma)\bar{a}$ geometry) with two maxima at ~ 514 and 542 cm^{-1} – to O vibrations. Note that the energy of the most intense mode is very different from the case of the isostructural SrLaAlO₄ crystal for which the two A_{1g} modes are at 222 (very intense) and 512 cm^{-1} (weak). Thus, we identify all 4 Raman-active modes. The bands at ~ 615 and 650 cm^{-1} are probably due to defect-induced modes [43].

4. Judd-Ofelt analysis

The absorption spectra of the Tm,Ho:Ca(Gd,Lu)AlO₄ crystal (batch #1) measured for π and σ light polarizations are shown in Fig. 10. The spectra contain bands assigned to Tm³⁺ dopant ions (the transitions from the ³H₆ ground-state to the excited-states from ³F₄ to ¹D₂), as well as Ho³⁺ ones (the transitions from the ⁵I₈ ground-state to the excited-states from ⁵I₇ to ³H₆). In Fig. 10, the assignment of the Ho³⁺ multiplets is after [46]. In the UV, the sharp lines at 302 - 314 nm are due to optical absorption of the host-forming cations (Gd³⁺, the ⁸S_{7/2} → ⁶P_{7/2} transition). The Lu³⁺ ions are optically inactive. In the visible, there is a broad structureless absorption band spanning from ~ 300 to 550 nm underlying the absorption of rare-earth ions. It is related to residual absorption of color centers.

The transition intensities of the Tm³⁺ ion in Ca(Gd,Lu)AlO₄ crystals have been already analyzed [28]. In the present work, we focus on the Ho³⁺ ion. For this, the known absorption due to Tm³⁺ was subtracted from the spectra shown in Fig. 10. The Judd-Ofelt (J-O) formalism was applied to electric-dipole (ED) contributions to transition intensities. The contribution of magnetic-dipole (MD) transitions (for $\Delta J = J - J' = 0, \pm 1$, except for $J = J' = 0$) was calculated separately within the Russell–Saunders approximation on wave functions of Ho³⁺ under an assumption of a free-ion. The set of reduced squared matrix elements $U^{(k)}$ was taken from [47]. The dispersion curves of CaGdAlO₄ reported in [8] were used. All the values were considered as polarization-averaged, $\langle \dots \rangle = (2\sigma + \pi)/3$.

The absorption oscillator strengths were determined from the measured absorption spectra using:

$$\langle f_{\text{exp}}(JJ') \rangle = \frac{m_e c^2}{\pi e^2 N_{\text{Ho}} \langle \lambda \rangle^2} \langle \Gamma(JJ') \rangle, \quad (2)$$

where m_e and e are the electron mass and charge, respectively, c is the speed of light, $\langle \Gamma(JJ') \rangle$ is the integrated absorption coefficient within the absorption band and $\langle \lambda \rangle$ is the “center of gravity” of the absorption band. The results are shown in Table 5.

In the standard J-O theory, the ED line strengths of the $J \rightarrow J'$ transitions $S^{\text{ED}}(JJ')$ are given by [48,49]:

$$S_{\text{calc}}^{\text{ED}}(JJ') = \sum_{k=2,4,6} U^{(k)} \Omega_k, \quad (3a)$$

$$U^{(k)} = \langle (4f^n)SLJ || U^{(k)} || (4f^n)S'L'J' \rangle^2. \quad (3b)$$

Here, $U^{(k)}$ are the reduced squared matrix elements and Ω_k are the intensity (J–O) parameters ($k=2, 4, 6$).

Let us take into account the possible configuration interaction. If only the lower-energy excited configuration of the opposite parity ($4f^{n-1}5d^1 = 4f^9 5d^1$ for Ho^{3+}) contributes to the configuration interaction, the ED line strengths are [50]:

$$S_{\text{calc}}^{\text{ED}}(JJ') = \sum_{k=2,4,6} U^{(k)} \tilde{\Omega}_k, \quad (4a)$$

$$\tilde{\Omega}_k = \Omega_k [1 + 2\alpha(E_J + E_{J'} - 2E_f^0)]. \quad (4b)$$

Here, the intensity parameters $\tilde{\Omega}_k$ are the linear functions of energies (E_J and $E_{J'}$) of the two multiplets involved in the transition $J \rightarrow J'$, E_f^0 is the mean energy of the $4f^n$ configuration and $\alpha \approx 1/(2\Delta)$, where Δ has the meaning of the average energy difference between the $4f^n$ and $4f^{n-1}5d^1$ configurations. This approximation is typically referred to as the modified Judd-Ofelt (mJ-O) theory [50,51]. The $\tilde{\Omega}_k$ parameters for the mJ-O theory are transformed into Ω_k ones for the standard theory assuming a high-lying $4f^{n-1}5d^1$ excited electronic configuration (i.e., the energy difference $\Delta \rightarrow \infty$ or, equivalently, $\alpha \rightarrow 0$).

The absorption oscillator strengths are related to the line strengths:

$$f_{\text{calc}}^{\Sigma}(JJ') = \frac{8}{3h(2J+1)\langle \lambda \rangle} \frac{(n^2+2)^2}{9n} S_{\text{calc}}^{\text{ED}}(JJ') + f_{\text{calc}}^{\text{MD}}(JJ'), \quad (5)$$

where h is the Planck constant, n is the refractive index of the crystal at $\langle \lambda \rangle$ and the superscript “ Σ ” stands for the total (ED + MD) value. In the standard J-O theory, there are three free parameters, ($\Omega_2, \Omega_4, \Omega_6$), and in the mJ-O theory, there are four free parameters, ($\Omega_2, \Omega_4, \Omega_6$ and α).

For the analysis, a total of 8 Ho^{3+} transitions in the $\text{Ca}(\text{Gd,Lu})\text{AlO}_4$ crystal were considered. The calculated absorption oscillator strengths are listed in Table 5. Both the J-O and the mJ-O theories provide close root-mean-square (r.m.s.) deviations between $\langle f_{\text{exp}} \rangle$ and \bar{f}_{calc} , namely 2.949 and 3.025, respectively. However, the latter theory better describes the transition to the metastable Ho^{3+} excited-state (5I_7), compare $\langle f_{\text{exp}} \rangle = 2.808 \times 10^{-6}$ with $\bar{f}_{\text{calc}} = 5.027 \times 10^{-6}$ (J-O) and 4.265×10^{-6} (mJ-O). Thus, it was selected for further analysis.

The obtained intensity parameters are listed in Table 6. For the mJ-O theory, they are $\Omega_2 = 11.221$, $\Omega_4 = 13.586$ and $\Omega_6 = 6.048$ [10^{-20} cm^2] and $\alpha = 0.070$ [10^{-4} cm], and the phenomenological parameter $\Delta = 1/(2\alpha) = 14.3 \times 10^4 \text{ cm}^{-1}$ (high-lying excited configuration).

The probabilities of radiative spontaneous transitions for emission channels $J \rightarrow J'$ are then determined from the corresponding line strengths in emission:

$$A_{\text{calc}}^{\Sigma}(JJ') = \frac{64\pi^4 e^2}{3h(2J+1)\langle \lambda \rangle^3} n \left(\frac{n^2+2}{3} \right)^2 S_{\text{calc}}^{\text{ED}}(JJ') + A_{\text{calc}}^{\text{MD}}(JJ'). \quad (6)$$

Using the A_{calc} values, we have further determined the total probabilities of spontaneous radiative transitions from the excited states A_{tot} , the corresponding radiative lifetimes τ_{rad} and the luminescence branching ratios for the particular emission channels $B(JJ')$:

$$\tau_{\text{rad}} = \frac{1}{A_{\text{tot}}}, \text{ where } A_{\text{tot}} = \sum_{J'} A_{\text{calc}}^{\Sigma}(JJ'); \quad (7a)$$

$$B(JJ') = \frac{A_{\text{calc}}^{\Sigma}(JJ')}{A_{\text{tot}}}, \quad (7b)$$

The results are shown in Table 7. They are obtained using the mJ-O theory. For the 5I_7 Ho³⁺ multiplet, τ_{rad} is 3.32 ms. Considering the residual difference between the $\langle f_{\text{exp}} \rangle$ and \bar{f}_{calc} values for the $^5I_8 \rightarrow ^5I_7$ transition in absorption, the upper limit for the estimated radiative lifetime of the 5I_7 state is 5.04 ms.

Previously, for the Ho:CaGdAlO₄ crystal, the following J-O parameters were reported: $\Omega_2 = 3.65$, $\Omega_4 = 3.79$ and $\Omega_6 = 4.17$ [10^{-20} cm²] [18] leading to the radiative lifetime of the 5I_7 state of 3.84 ms which reasonably agrees with our data.

5. Conclusions

To conclude, we explored the formation of substitutional solid-solutions in the system CaGd_{1-x}Lu_xAlO₄ as laser host materials for doping with laser-active Tm³⁺ and Ho³⁺ ions. The crystals of Tm,Ho:Ca(Gd,Lu)AlO₄ with Lu³⁺ content up to 10.8 at.% (which is almost twice higher than in the previous studies for other laser-active rare-earth dopants) are grown by the Cz method using [001]-oriented seeds from CaGdAlO₄. The segregation coefficients for rare-earth ions (Lu³⁺, Tm³⁺ and Ho³⁺) are determined and correlated with their ionic radii suggesting an empirical formula. The Tm,Ho:Ca(Gd,Lu)AlO₄ crystals maintain the tetragonal (K₂NiF₄-type, sp. gr. *I4/mmm*) structure. The Rietveld refinement data include the fractional atomic coordinates and interatomic distances. The first (by oxygen) and second (by Ca²⁺|RE³⁺ cations) coordination spheres of rare-earth sites are described. The low-phonon-energy vibronic behavior of Tm,Ho:Ca(Gd,Lu)AlO₄ crystals is revealed. The most intense Raman mode is found at 311 cm⁻¹ (assigned to A_{1g} symmetry) and the maximum phonon frequency is ~650 cm⁻¹. The polarized absorption spectra of Tm,Ho:Ca(Gd,Lu)AlO₄ crystals are systematically studied. The Ho³⁺ transition probabilities are described using the modified Judd-Ofelt (mJ-O) theory accounting for the configuration interaction.

Future work regarding the growth of rare-earth-doped Ca(Gd,Lu)AlO₄ crystals should focus on exploiting the limit of stability of the CaGd_{1-x}Lu_xAlO₄ solution. In the present work, using the Goldschmidt's tolerance factor *t* modified for the ABCO₄ structure, we estimated the upper limit of stability to be $x \sim 0.7$. The introduction of even higher Lu³⁺ content may greatly promote the spectral broadening for dopant ions and facilitate their segregation factors (as the difference of ionic radii of Yb³⁺|Tm³⁺|Ho³⁺ and Lu³⁺ is smaller as compared with Gd³⁺). Indeed, in the present work, the introduction of 10.8 at.% Lu³⁺ resulted in increased Tm³⁺ segregation coefficient $K_{\text{Tm}} = 0.90$, compared with its value of ~0.6 for the parent compound, CaGdAlO₄.

Acknowledgments

This work was supported by the Spanish Government, Ministry of Science and Innovation (project No. PID2019-108543RB-I00) and by the Generalitat de Catalunya (project No. 2017SGR755).

References

1. J. Petit, P. Goldner, B. Viana, Laser emission with low quantum defect in Yb:CaGdAlO₄, Opt. Lett. 30 (2005) 1345-1347.
2. J.A. Hutchinson, H.R. Verdun, B.H. Chai, B. Zandi, L.D. Merkle, Spectroscopic evaluation of CaYAIO₄ doped with trivalent Er, Tm, Yb and Ho for eyesafe laser applications, Opt. Mater. 3 (1994) 287-306.

3. R. Moncorgé, N. Garnier, P. Kerbrat, C. Wyon, C. Borel, Spectroscopic investigation and two-micron laser performance of Tm³⁺:CaYAlO₄ single crystals, *Opt. Commun.* 141 (1997) 29-34.
4. R.D.Shannon, R.A. Oswald, J.B. Parise, B.H.T. Chai, P. Byszewski, A. Pajaczkowska, R. Sobolewski, Dielectric constants and crystal structures of CaYAlO₄, CaNdAlO₄, and SrLaAlO₄, and deviations from the oxide additivity rule, *J. Sol. State Chem.* 98 (1992) 90-98.
5. L. Vasylechko, N. Kodama, A. Matkovskii, Y. Zhydachevskii, Crystal structure and optical spectroscopy of CaGdAlO₄:Er single crystal, *J. Alloys Compd.* 300 (2000) 475-478.
6. P.O. Petit, J. Petit, P. Goldner, B. Viana, Inhomogeneous broadening of optical transitions in Yb:CaYAlO₄, *Opt. Mater.* 30 (2008) 1093-1097.
7. P. Loiko, F. Druon, P. Georges, B. Viana, K. Yumashev, Thermo-optic characterization of Yb:CaGdAlO₄ laser crystal, *Opt. Mater. Express* 4 (2014) 2241-2249.
8. P. Loiko, P. Becker, L. Bohatý, C. Liebald, M. Peltz, S. Vernay, D. Rytz, J. M. Serres, X. Mateos, Y. Wang, X. Xu, J. Xu, A. Major, A. Baranov, U. Griebner, V. Petrov, Sellmeier equations, group velocity dispersion and thermo-optic dispersion formulas for CaLnAlO₄ (Ln =Y, Gd) laser host crystals, *Opt. Lett.* 42 (2017) 2275-2278.
9. P. Loiko, J.M. Serres, X. Mateos, X. Xu, J. Xu, V. Jambunathan, P. Navratil, A. Lucianetti, T. Mocek, X. Zhang, U. Griebner, V. Petrov, M. Aguiló, F. Díaz, A. Major, Microchip Yb:CaLnAlO₄ lasers with up to 91% slope efficiency, *Opt. Lett.* 42 (2017) 2431-2434.
10. D. Li, X. Xu, Y. Cheng, S. Cheng, D. Zhou, F. Wu, C. Xia, J. Xu, J. Zhang, Crystal growth and spectroscopic properties of Yb:CaYAlO₄ single crystal, *J. Cryst. Growth* 312 (2010) 2117-2121.
11. Y. Zaouter, J. Didierjean, F. Balembois, G. Lucas Leclin, F. Druon, P. Georges, J. Petit, P. Goldner, B. Viana, 47-fs diode-pumped Yb³⁺:CaGdAlO₄ laser, *Opt. Lett.* 31 (2006) 119-121.
12. P. Sévillano, P. Georges, F. Druon, D. Descamps, E. Cormier, 32-fs Kerr-lens mode-locked Yb:CaGdAlO₄ oscillator optically pumped by a bright fiber laser, *Opt. Lett.* 39 (2014) 6001-6004.
13. F. Druon, M. Olivier, A. Jaffrès, P. Loiseau, N. Aubry, J. DidierJean, F. Balembois, B. Viana, P. Georges, Magic mode switching in Yb:CaGdAlO₄ laser under high pump power, *Opt. Lett.* 38 (2013) 4138-4141.
14. K. Beil, B. Deppe, C. Kränkel, Yb:CaGdAlO₄ thin-disk laser with 70% slope efficiency and 90 nm wavelength tuning range, *Opt. Lett.* 38 (2013) 1966-1968.
15. A. Diebold, F. Emaury, C. Schriber, M. Golling, C.J. Saraceno, T. Südmeyer, U. Keller, SESAM mode-locked Yb:CaGdAlO₄ thin disk laser with 62 fs pulse generation, *Opt. Lett.* 38 (2013) 3842-3845.
16. Y. Wang, G. Xie, X. Xu, J. Di, Z. Qin, S. Suomalainen, M. Guina, A. Härkönen, A. Agnesi, U. Griebner, X. Mateos, P. Loiko, V. Petrov, SESAM mode-locked Tm:CALGO laser at 2 μm, *Opt. Mater. Express* 6 (2016) 131-136.
17. Y. Zhao, Y. Wang, X. Zhang, X. Mateos, Z. Pan, P. Loiko, W. Zhou, X. Xu, J. Xu, D. Shen, S. Suomalainen, A. Härkönen, M. Guina, U. Griebner, V. Petrov, 87 fs mode-locked Tm, Ho:CaYAlO₄ laser at ~2043 nm, *Opt. Lett.* 43 (2018) 915-918.
18. J. Di, X. Xu, C. Xia, Q. Sai, D. Zhou, Z. Lv, J. Xu, Growth and spectra properties of Tm, Ho doped and Tm, Ho co-doped CaGdAlO₄ crystals, *J. Lumin.* 155 (2014) 101-107.
19. A. Pajaczkowska, A. Gloubokov, Synthesis, growth and characterization of tetragonal ABCO₄ crystals, *Prog. Cryst. Growth Charact. Mater.* 36 (1998)123-162.
20. Z. Pan, X. Dai, Y. Lei, H. Cai, J.M. Serres, M. Aguiló, F. Díaz, J. Ma, D. Tang, E. Vilejshikova, U. Griebner, V. Petrov, P. Loiko, X. Mateos, Crystal growth and properties of the disordered crystal Yb:SrLaAlO₄: a promising candidate for high-power ultrashort pulse lasers, *CrystEngComm* 20 (2018) 3388-3395.
21. A. Dabkowski, H.A. Dabkowski, J.E. Greedan, SrLaGaO₄-Czochralski crystal growth and basic properties, *J. Cryst. Growth* 132 (1993) 205-208.
22. A. Novoselov, G. Zimina, L. Komissarova, A. Pajaczkowska, Synthesis and characterization of solid solutions in ABCO₄ system. *J. Cryst. Growth*, 287 (2006) 305-308.
23. F. Guo, Q. Xie, L. Qiu, B. Zhao, X. Chen, J. Chen, Growth, magnetic and magneto-optical properties of CaDyAlO₄ crystals, *Opt. Mater.* 112 (2021) 110719.
24. M. Mei, L.L. Cao, Y. He, R.R. Zhang, F.Y. Guo, N.F. Zhuang, J.Z. Chen, Growth and magneto-optical properties of CaTbAlO₄ crystal, *Adv. Mater. Res.* 306 (2011) 1722-1727.

25. K. Beil, S.T. Fredrich-Thornton, F. Tellkamp, R. Peters, C. Kränkel, K. Petermann, G. Huber, Thermal and laser properties of Yb:LuAG for kW thin disk lasers, *Opt. Express* 18 (2010) 20712-20722.
26. C. Liebald, Yb-dotierte Ultrakurzpuls-Lasermaterialien mit K_2NiF_4 -Struktur - Züchtung und Verbesserung der Kristallqualität (Doctoral dissertation, Johannes Gutenberg-Universität Mainz, 2017) [in German].
27. Q. Hu, Z. Jia, A. Volpi, S. Veronesi, M. Tonelli, X. Tao, Crystal growth and spectral broadening of a promising Yb:CaLu_xGd_{1-x}AlO₄ disordered crystal for ultrafast laser application, *CrystEngComm* 19 (2017) 1643-1647.
28. Z. Pan, P. Loiko, J.M. Serres, E. Kifle, H. Yuan, X. Dai, H. Cai, Y. Wang, Y. Zhao, M. Aguiló, F. Díaz, U. Griebner, V. Petrov, X. Mateos, "Mixed" Tm:Ca(Gd,Lu)AlO₄ — a novel crystal for tunable and mode-locked 2 μ m lasers," *Opt. Express* 27 (2019) 9987-9995.
29. H. Bernhardt, On the coloration behaviour of undoped YAlO₃ crystals, *Phys. Stat. Sol. A* 21 (1974) 95-98.
30. Q. Hu, Z. Jia, C. Tang, N. Lin, J. Zhang, N. Jia, S. Wang, X. Zhao, X. Tao, The origin of coloration of CaGdAlO₄ crystals and its effect on their physical properties, *CrystEngComm* 19 (2017) 537-545.
31. A. Pajaczkowska, A. Gloubokov, A. Klos, C.F. Woensdregt, Czochralski growth of SrLaAlO₄ and SrLaGaO₄ single crystals and its implications for the crystal morphology, *J. Cryst. Growth* 171 (1997) 387-391.
32. R.D. Shannon, Revised effective ionic radii and systematic studies of interatomic distances in halides and chalcogenides, *Acta Cryst. A* 32 (1976) 751-767.
33. J. Di, X. Sun, X. Xu, C. Xia, Q. Sai, H. Yu, Y. Wang, L. Zhu, Y. Gao, X. Guo, Growth and spectral characters of Nd:CaGdAlO₄ crystal, *Eur. Phys. J. Appl. Phys.* 74 (2016) 10501.
34. Q. Hu, Z. Jia, S. Veronesi, J. Zhang, A. Sottile, M. Tonelli, E. Cavalli, X. Tao, Crystal growth and optimization of Pr:CaGdAlO₄ by the flux-Czochralski method, *CrystEngComm* 20 (2018) 590-596.
35. R. Li, X. Xu, L. Su, Q. Sai, C. Xia, Q. Yang, J. Xu, A. Strzyp, A. Półkoszek, Crystal characterization and optical spectroscopy of Eu³⁺-doped CaGdAlO₄ single crystal fabricated by the floating zone method, *Chin. Opt. Lett.* 14 (2016) 021602.
36. S. Li, Y. Yang, S. Zhang, T. Yan, N. Ye, Y. Hang, Enhanced 2.86 μ m emission from a Ho, Pr:CaGdAlO₄ crystal, *J. Lumin.* 228 (2020) 117620.
37. N. Zhang, H. Wang, Y. Yin, T. Wang, Z. Jia, J. Zhang, Q. Hu, N. Lin, X. Fu, X. Tao, Cracking mechanism and spectral properties of Er, Yb:CaGdAlO₄ crystals grown by the LHPG method, *CrystEngComm* 22 (2020) 955-960.
38. K. Hasse, T. Calmano, B. Deppe, C. Liebald, C. Kränkel, Efficient Yb³⁺:CaGdAlO₄ bulk and femtosecond-laser-written waveguide lasers, *Opt. Lett.* 40 (2015) 3552-3555.
39. K. Subbotin, P. Loiko, S. Slimi, A. Volokitina, A. Titov, D. Lis, E. Chernova, S. Kuznetsov, R.M. Solé, U. Griebner, V. Petrov, M. Aguiló, F. Díaz, P. Camy, E. Zharikov, X. Mateos, Monoclinic zinc monotonungstate Yb³⁺,Li⁺:ZnWO₄: Part I. Czochralski growth, structure refinement and Raman spectra, *J. Lumin.* 228 (2020) 117601.
40. I. Zvereva, Y. Smirnov, J. Choisnet, Demixion of the K_2NiF_4 type aluminate LaCaAlO₄: precursor role of the local ordering of lanthanum and calcium, *Mater. Chem. Phys.* 60 (1999) 63-69.
41. V.M. Goldschmidt, Die Gesetze der Kristallochemie, *Naturwissenschaften* 21 (1926) 477-485.
42. D.L. Rousseau, R.P. Bauman, S.P.S. Porto, Normal mode determination in crystals, *J. Raman Spectr.* 10 (1981) 253-290.
43. V.G. Hadjiev, M. Cardona, I. Ivanov, V. Popov, M. Gyulmezov, M.N. Iliev, M. Berkowski, Optical phonons probe of the SrLaAlO₄ crystal structure, *J. Alloy Compd.* 251 (1997) 7-10.
44. A.A. Kaminskii, X. Xu, O. Lux, H. Rhee, H.J. Eichler, J. Zhang, D. Zhou, A. Shirakawa, K. Ueda, J. Xu, High-order stimulated Raman scattering in tetragonal CaYAlO₄ crystal-host for Ln³⁺-lasant ions, *Laser Phys. Lett.* 9 (2012) 306-311.
45. T.C. Damen, S.P.S. Porto, B. Tell, Raman effect in zinc oxide, *Phys. Rev.* 142 (1966) 570-574.
46. W.T. Carnall, P.R. Fields, K. Rajnak, Electronic energy levels in the trivalent lanthanide aquo ions. I. Pr³⁺, Nd³⁺, Pm³⁺, Sm³⁺, Dy³⁺, Ho³⁺, Er³⁺, and Tm³⁺, *J. Chem. Phys.* 49 (1968) 4424-4442.
47. M.C. Pujol, C. Cascales, M. Rico, J. Massons, F. Diaz, P. Porcher, C. Zaldo, Measurement and crystal field analysis of energy levels of Ho³⁺ and Er³⁺ in KGd(WO₄)₂ single crystal, *J. Alloys Compd.* 323 (2001) 321-325.

48. B.R. Judd, Optical absorption intensities of rare-earth ions, *Phys. Rev.* 127 (1962) 750–761.
49. G.S. Ofelt, Intensities of crystal spectra of rare-earth ions, *J. Chem. Phys.* 37 (1962) 511–520.
50. A.A. Kornienko, A.A. Kaminskii, E.B. Dunina, Dependence of the line strength of f–f transitions on the manifold energy. II. Analysis of Pr^{3+} in $\text{KPrP}_4\text{O}_{12}$, *Phys. Stat. Sol. B* 157 (1990) 267-273.
51. P. Loiko, A. Volokitina, X. Mateos, E. Dunina, A. Kornienko, E. Vilejshikova, M. Aguilo, F. Diaz, Spectroscopy of Tb^{3+} ions in monoclinic $\text{KLu}(\text{WO}_4)_2$ crystal: application of an intermediate configuration interaction theory, *Opt. Mater.* 78 (2018) 495-501.

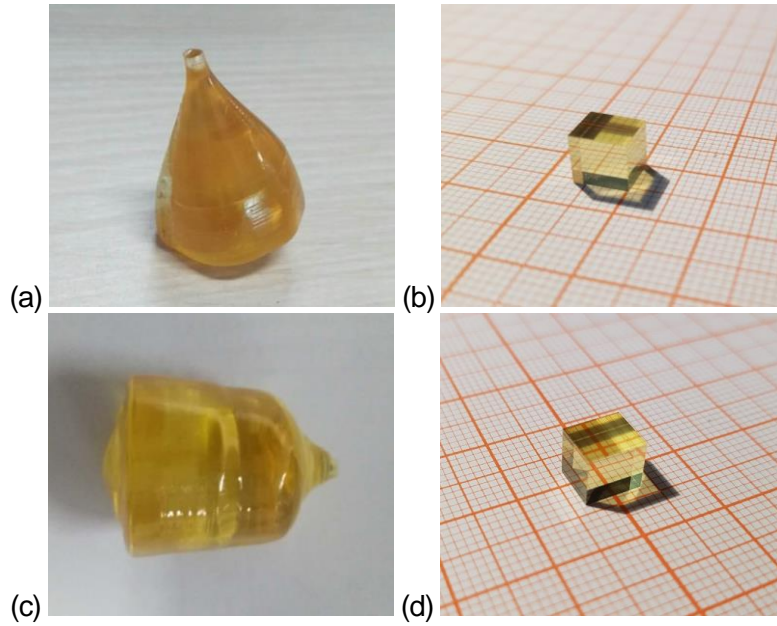


Fig. 1. (a-d) Photographs of the Tm,Ho:Ca(Gd,Lu)AlO₄ crystals grown by the Czochralski method: (a,c) as-grown crystal boules, (b,d) polished cubic samples oriented along crystallographic axes; (a,b) 5.5 at.% Lu³⁺, (c,d) 10.8 at.% Lu³⁺ (in the crystal). The full chemical formulas are given in Table 1. The growth direction is along the [001] axis.

Table 1. Raw and actual compositions of the Tm,Ho:Ca(Gd,Lu)AlO₄ crystals grown by the Czochralski method, K_{RE} – segregation coefficient.

Crystal	Batch #1	Batch #2
Raw composition		
Tm, at.%	5.0	5.0
Ho, at.%	0.5	0.5
Lu, at.%	10.0	20.0
Actual composition		
Tm, at.% [cm ⁻³]	4.48 [5.54×10 ²⁰]	4.50 [5.55×10 ²⁰]
Ho, at.% [cm ⁻³]	0.54 [0.66×10 ²⁰]	0.38 [0.47×10 ²⁰]
Lu, at.% [cm ⁻³]	5.51 [6.78×10 ²⁰]	10.80 [13.3×10 ²⁰]
Chemical formula	CaGd _{0.8946} Lu _{0.055} Tm _{0.045} Ho _{0.0054} AlO ₄	CaGd _{0.8327} Lu _{0.108} Tm _{0.0555} Ho _{0.0038} AlO ₄
K_{Tm}	0.90	0.90
K_{Ho}	1.07	0.76
K_{Lu}	0.55	0.54

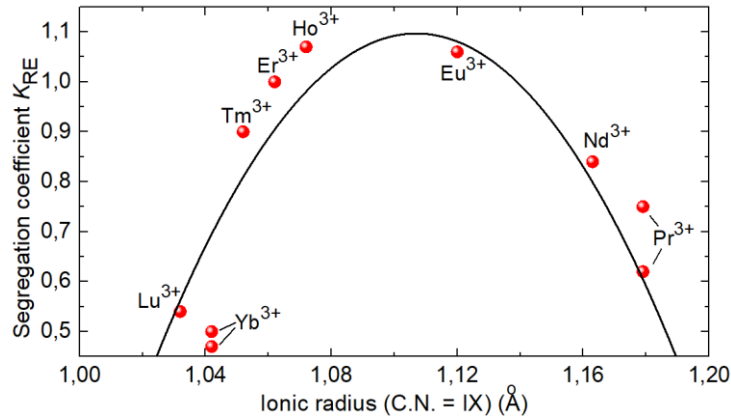


Fig. 2. Segregation coefficients of rare-earth ions (RE^{3+}) K_{RE} in $CaGdAlO_4$ crystals vs. their ionic radii for VIX-fold oxygen coordination (C.N. – coordination number), *circles* - experimental data (this work and Refs. [33-38]), *curve* – their fit according to the Onuma's principle [39], $K_{RE} = K_0 - C(R_{RE} - R_{Gd})^2$ where $K_0 = 1.1 \pm 0.1$ and $C = 95 \pm 5 \text{ \AA}^{-2}$ (this work).

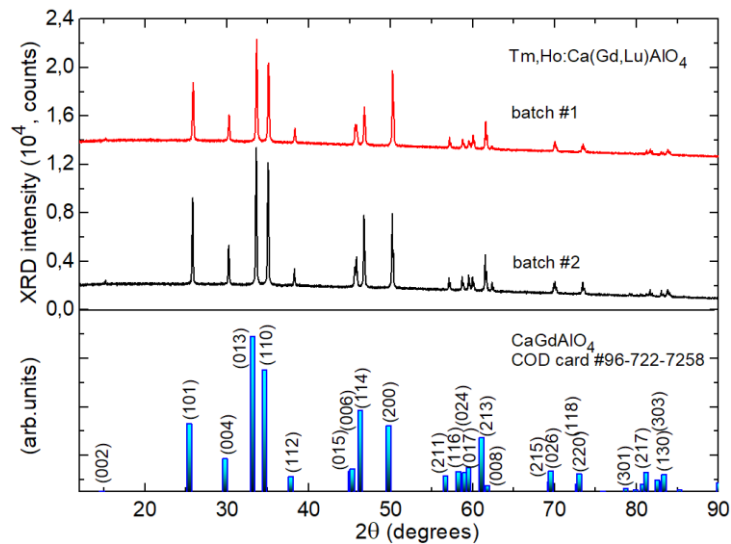


Fig. 3. X-ray powder diffraction (XRD) patterns of $Tm, Ho:Ca(Gd, Lu)AlO_4$ crystals, *vertical bars* mark theoretical reflections for undoped $CaGdAlO_4$ (COD card #96-722-7258), *numbers* indicate the Miller's indices (hkl).

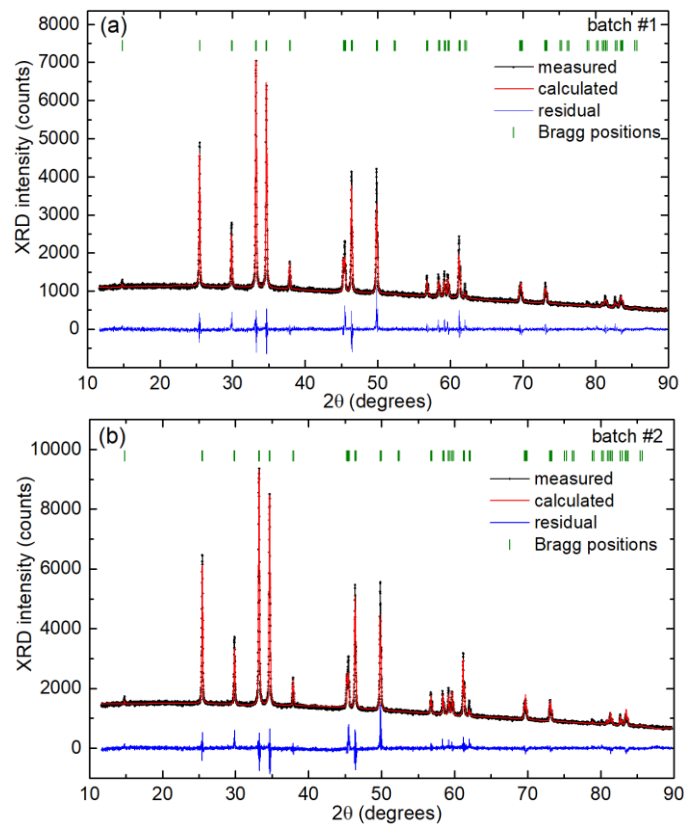


Fig. 4. (a,b) Rietveld refinement of the XRD patterns of $Tm, Ho:Ca(Gd, Lu)AlO_4$ crystals: observed (*black*), calculated (*red*) and differential (*blue*) patterns, *vertical dashes* – Bragg reflections (*green*), growth batch: (a) #1 and (b) #2, cf. Table 1.

Table 2. Crystallographic data and Rietveld refinement parameters for Tm,Ho:Ca(Gd,Lu)AlO₄ crystals.

Parameter	Value
System	Tetragonal
Space group (IT number)	$D_{4h}^{17} - I4/mmm$ (No. 139)
Number of formula units	$Z = 2$
Point Group	$4/mmm$
Reduced Number of S.O.	8
General multiplicity	32
Centrosymmetry	Centric (-1 at origin)
Calculated density (g/cm ³)	6.010 (#1) 6.028 (#2)
Lattice constants a, c (Å)	3.6585 (6), 11.9660 (9) (#1) 3.6592 (4), 11.9689 (1) (#2)
$\alpha = \beta = \gamma$ (deg.)	90
Volume (Å ³)	160.167 (#1) 160.264 (#2)
2θ range (deg)	12-90
2θ step	0.02
Radiation	Cu-K α 1 ($\lambda = 1.5418$ Å)
No. of reflections	72
Refinement software	<i>match!</i> software
Reliability factors	$R_p = 2.82, R_{wp} = 4.22,$ $R_{exp} = 2.31$ and $\chi^2 = 3.33$ (#1) $R_p = 2.57, R_{wp} = 3.87,$ $R_{exp} = 2.31$ and $\chi^2 = 2.80$ (#2)

Table 3. Atomic coordinates (x, y, z), occupancy factors (O.F.) and isotropic displacement parameters B_{iso} determined via Rietveld refinement for Tm,Ho:Ca(Gd,Lu)AlO₄ crystals.

Atoms	Site	x	y	z	O.F.	$B_{iso}, \text{Å}^2$
Batch #1						
Ca	4e	1/2	1/2	0.1402 (0)	0.500	2.089
Gd Lu	4e	1/2	1/2	0.1402 (0)	0.447 0.027	2.089
Tm Ho	4e	1/2	1/2	0.1402 (0)	0.022 0.002	2.089
Al	2a	0	0	0	1	0.467
O1	4e	1/2	1/2	0.3304 (0)	1	1.842
O2	4c	0	1/2	0	1	1.863
Batch #2						
Ca	4e	1/2	1/2	0.1404 (0)	0.500	2.362
Gd Lu	4e	1/2	1/2	0.1404 (0)	0.416 0.054	2.362
Tm Ho	4e	1/2	1/2	0.1404 (0)	0.027 0.001	2.362
Al	2a	0	0	0	1	0.763
O1	4e	1/2	1/2	0.3317 (0)	1	2.730
O2	4c	0	1/2	0	1	1.980

Table 4. Selected interatomic distances for Tm,Ho:Ca(Gd,Lu)AlO₄ crystals.

Distances	Value (Å)	
	Batch #1	Batch #2
Al – O	O2 1.829(2) ×4	O2 1.829(6) ×4
	O1 2.028(4) ×2	O1 2.013(6) ×2
Ca RE – O	O1 2.276(9) ×1	O1 2.289(8) ×1
	O2 2.482(0) ×4	O2 2.484(5) ×4
	O1' 2.610(6) ×4	O1' 2.608(7) ×4
Ca RE – Ca RE	3.355(2) ×1	3.361(8) ×1
	3.658(5) ×4	3.659(2) ×4
	3.687(5) ×4	3.684(1) ×4

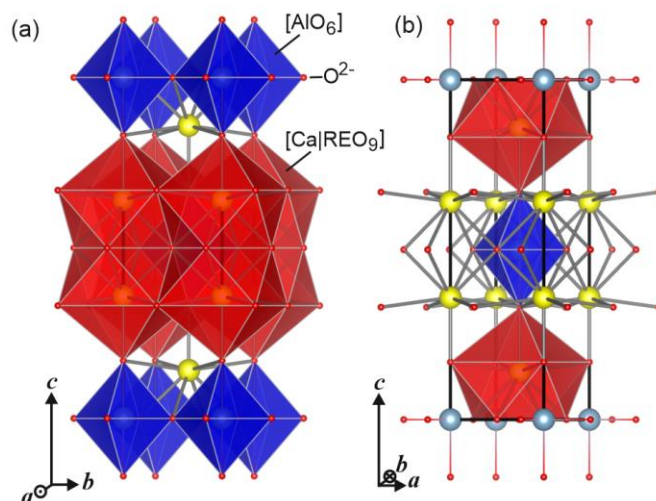


Fig. 5. Fragment of the structure of a Tm,Ho:Ca(Gd,Lu)AlO₄ crystal, *black lines* mark the unit-cell, blue polyhedra – [AlO₆] and red polyhedra – [Ca|REO₉], where RE = Gd, Lu, Tm or Ho.

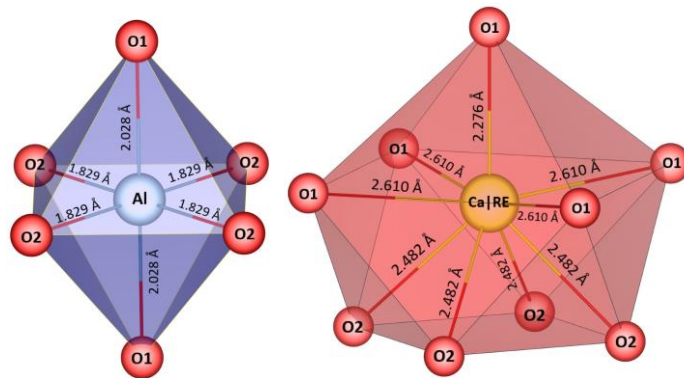


Fig. 6. Schematic of the [AlO₆] (left) and [Ca|REO₉] (right) polyhedra in the structure of Tm,Ho:Ca(Gd,Lu)AlO₄ (batch #1).

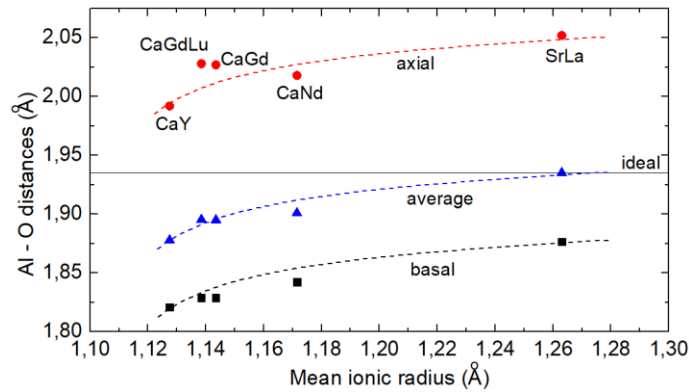


Fig. 7. Al – O interatomic distances in [AlO₆] octahedra for MM'AlO₄ crystals with K₂NiF₄-type structure versus the mean ionic radius of M²⁺ and M³⁺ cations (the data from the present work and Ref. [4]). Horizontal line – ideal Al – O distance calculated from the ionic radii of VI-fold coordinated Al³⁺ and O²⁻.

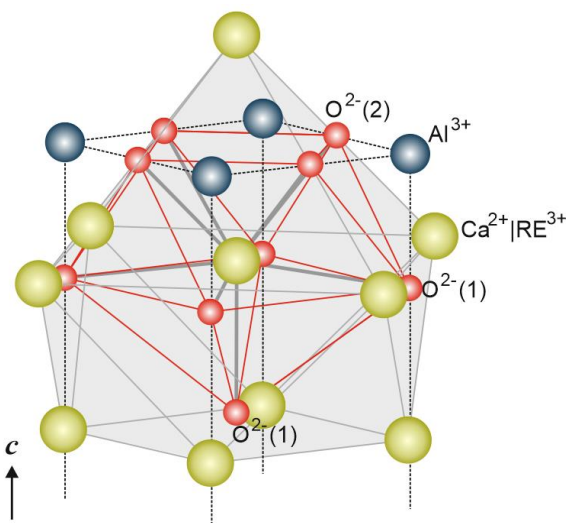


Fig. 8. Second coordination sphere of Tm³⁺|Ho³⁺ ions by Ca²⁺|RE³⁺ cations in Tm,Ho:Ca(Gd,Lu)AlO₄.

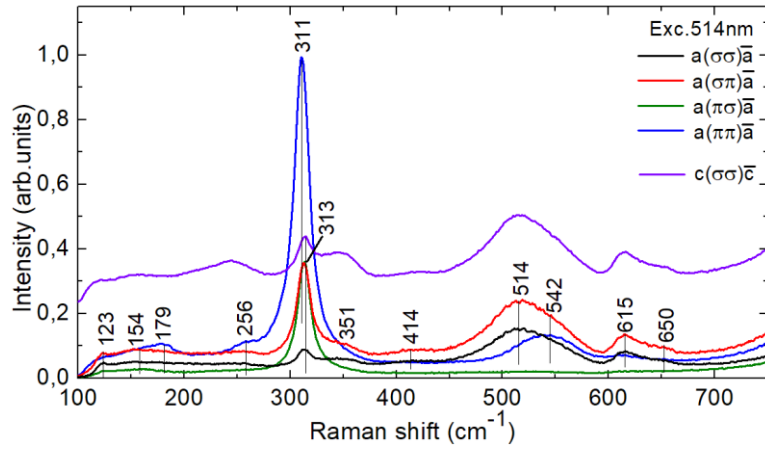


Fig. 9. Polarized Raman spectra of *a*-cut and *c*-cut Tm,Ho:Ca(Gd,Lu)AlO₄ crystals (batch #1) (Porto's notations), $\lambda_{\text{exc}} = 514 \text{ nm}$, numbers – Raman frequencies in cm^{-1} .

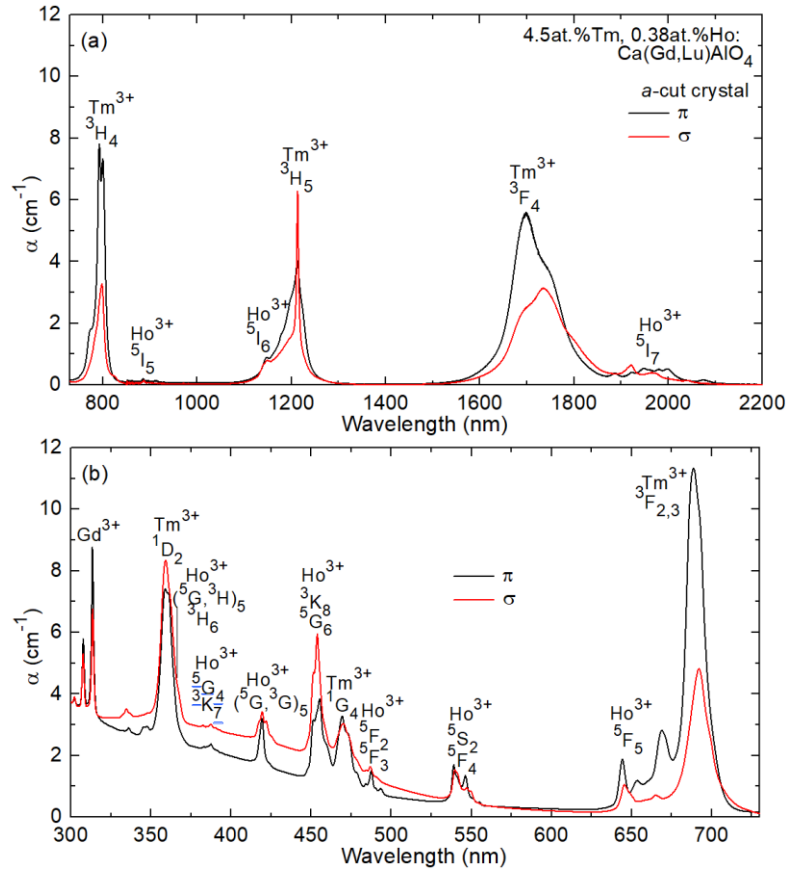


Fig. 10. Polarized absorption spectra of a Tm,Ho:Ca(Gd,Lu)AlO₄ crystal (batch #1) for π and σ light polarizations: (a) near-IR, (b) visible and UV.

Table 5. Experimental and calculated absorption oscillator strengths* for Ho³⁺ ions in Tm,Ho:Ca(Gd,Lu)AlO₄ crystals.

⁵ I ₈ → ² S+ ¹ L _J	<λ>, nm	<Γ>, cm ⁻¹ nm	<f _{exp} >, 10 ⁻⁶	f ^Σ _{calc} , 10 ⁻⁶	
				J-O	mJ-O
⁵ I ₇	1935	37.27	2.808	4.459 ^{ED+} 0.568 ^{MD}	3.697 ^{ED+} 0.568 ^{MD}
⁵ I ₆	1162	30.34	5.156	3.049 ^{ED}	2.829 ^{ED}
⁵ I ₅	898	2.03	0.610	0.585 ^{ED}	0.568 ^{ED}
⁵ F ₅	772	30.75	16.835	12.391 ^{ED}	11.367 ^{ED}
⁵ S ₂ + ⁵ F ₄	656	13.81	11.327	13.430 ^{ED}	14.187 ^{ED}
⁵ F ₃ + ⁵ F ₂ + ³ K ₈ + ⁵ G ₆	544	56.36	62.272	63.291 ^{ED+} 0.126 ^{MD}	62.984 ^{ED+} 0.126 ^{MD}
⁵ G ₁₅	467	9.81	13.455	16.470 ^{ED}	16.015 ^{ED}
⁵ G ₂₅ + ³ H ₆ + ³ F ₂	422	13.20	24.592	19.528 ^{ED}	21.247 ^{ED}
<i>r.m.s. dev.</i>				2.949	3.025

*<λ> - "center of gravity" of an absorption band, <Γ> – integrated absorption coefficient, <f_{exp}> and f^Σ_{calc} – experimental and calculated absorption oscillator strengths, respectively, ED and MD stand for the electric-dipole and magnetic-dipole contributions, respectively, <> stand for polarization-averaging, (2σ + π)/3.

Table 6. Intensity parameters of Ho³⁺ ions in Ca(Gd,Lu)AlO₄.

Parameter	J-O theory	mJ-O theory
$\Omega_2 \times 10^{20}$, cm ²	8.899	11.221
$\Omega_4 \times 10^{20}$, cm ²	11.194	13.586
$\Omega_6 \times 10^{20}$, cm ²	3.685	6.048
$\alpha \times 10^4$, cm	-	0.070

Table 7. Calculated probabilities of spontaneous radiative transitions* of Ho³⁺ ions in Ca(Gd,Lu)AlO₄ (the mJ-O theory).

Emitting state	Terminal state	$\langle \lambda \rangle$, nm	$A_{\text{calc}}^{\Sigma}(\text{JJ}')$, s ⁻¹	$B(\text{JJ}')$	A_{tot} , s ⁻¹	τ_{rad} , ms
⁵ I ₇	⁵ I ₈	1935	273.0 ^{ED} +42.0 ^{MD}	1	301.5	3.32
⁵ I ₆	⁵ I ₇	2909	76.9 ^{ED} +20.4 ^{MD}	0.137	763.6	1.31
	⁵ I ₈	1162	654.6 ^{ED}	0.863		
⁵ I ₅	⁵ I ₆	3964	33.9 ^{ED} +9.5 ^{MD}	0.063	584.1	1.46
	⁵ I ₇	1678	364.8 ^{ED}	0.554		
	⁵ I ₈	898	262.9 ^{ED}	0.383		
⁵ I ₄	⁵ I ₅	5507	28.4 ^{ED} +4.2 ^{MD}	0.073	452.2	2.21
	⁵ I ₆	2305	177.2 ^{ED}	0.391		
	⁵ I ₇	1286	198.1 ^{ED}	0.451		
	⁵ I ₈	772	38.5 ^{ED}	0.085		
⁵ F ₅	⁵ I ₄	4354	0.5 ^{ED} +0.03 ^{MD}	<0.001	13235	0.076
	⁵ I ₅	2431	44.2 ^{ED} +0.8 ^{MD}	0.002		
	⁵ I ₆	1507	553.7 ^{ED} +2.8 ^{MD}	0.028		
	⁵ I ₇	993	2682 ^{ED}	0.171		
	⁵ I ₈	656	10230 ^{ED}	0.799		
⁵ S ₂ + ⁵ F ₄	⁵ F ₅	3191	57.7 ^{ED} +6.8 ^{MD}	<0.001	36993	0.021
	⁵ I ₄	1841	394.9 ^{ED} +0.07 ^{MD}	0.021		
	⁵ I ₅	1380	1125 ^{ED} +0.3 ^{MD}	0.019		
	⁵ I ₆	1023	3062 ^{ED}	0.078		
	⁵ I ₇	757	7490 ^{ED}	0.380		
	⁵ I ₈	544	24901 ^{ED}	0.502		

* $\langle \lambda \rangle$ - mean emission wavelength of the emission band, $A_{\text{calc}}^{\Sigma}(\text{JJ}')$ – probability of radiative spontaneous transition, $B(\text{JJ}')$ – luminescence branching ratio, A_{tot} and τ_{rad} – total probability of radiative spontaneous transitions and the radiative lifetime, respectively, ED and MD stand for the electric-dipole and magnetic-dipole contributions, respectively.